JGR Space Physics

RESEARCH ARTICLE
10.1029/2020JA028722

Key Points:

- An Magnetospheric Multiscale data base of current-sheet crossings was used to identify magnetopause crossings with the highest He^+ densities
- All of the high He^+ density crossings show evidence of plasmaspheric plume material, but only half are directly associated with a plasmaspheric plume
- The He^+ density varies dramatically in the magnetosphere, with order of magnitude variations as short as the time resolution of the composition instrument (10 s)
- The presence of high-density plasmaspheric plume material at the magnetopause produces transient reconnection rate reductions of up to ~40%

Correspondence to:
S. A. Fuselier,
stephen.fuselier@swri.org

Citation:
Fuselier, S. A., Haaland, S., Tenfjord, P., Paschmann, G., Toledo-Redondo, S., Malaspina, D., et al. (2021). High-density magnetospheric He^+ at the dayside magnetopause and its effect on magnetic reconnection. *Journal of Geophysical Research: Space Physics*, *126*, e2020JA028722. https://doi.org/10.1029/2020JA028722

Received 17 SEP 2020
Accepted 25 NOV 2020

High-Density Magnetospheric He^+ at the Dayside Magnetopause and Its Effect on Magnetic Reconnection

S. A. Fuselier[1,2], S. Haaland[3,4], P. Tenfjord[5], G. Paschmann[6], S. Toledo-Redondo[7], D. Malaspina[8,9], M. J. Kim[2,1], K. J. Trattner[9], S. M. Petrinec[10], B. L. Giles[11], J. Goldstein[1,2], J. L. Burch[1], and R. J. Strangeway[12]

[1]Southwest Research Institute, San Antonio, TX, USA, [2]Department of Physics and Astronomy, University of Texas at San Antonio, San Antonio, TX, USA, [3]Max-Planck-Institut für Sonnensystemforschung, Göttingen, Germany, [4]Birkeland Centre for Space Science, University of Bergen, Bergen, Norway, [5]Space Plasma Physics Group, University of Bergen, Bergen, Norway, [6]Max-Planck-Institut für extraterrestrische Physik, Garching, Germany, [7]Departament of Electromagnetism and Electronics, University of Murcia, Murcia, Spain, [8]Astrophysical and Planetary Sciences Department, University of Colorado, Boulder, CO, USA, [9]Laboratory for Atmospheric and Space Physics, University of Colorado Boulder, Boulder, CO, USA, [10]Lockheed Martin Advanced Technology Center, Palo Alto, CA, USA, [11]Goddard Space Flight Center, Greenbelt, MD, USA, [12]Institute of Geophysics and Planetary Physics, University of California, Los Angeles, CA, USA

Abstract Observations from the Magnetospheric Multiscale (MMS) mission are used to quantify the maximum effect of magnetospheric H^+ and He^+ on dayside magnetopause reconnection. A data base of current-sheet crossings from the first 2 years of the MMS mission is used to identify magnetopause crossings with the highest He^+ concentrations. While all of these magnetopause crossings exhibit evidence of plasmaspheric plume material, only half of the crossings are directly associated with plasmaspheric plumes. The He^+ density varies dramatically within the magnetosphere adjacent to the magnetopause, with density variations of an order of magnitude on timescales as short as 10 s, the time resolution of the composition instrument on MMS. Plasma wave observations are used to determine the total electron density, and composition measurements are used to determine the mass density in the magnetosheath and magnetosphere. These mass densities are then used with the magnetic field observations to determine the theoretical reduction in the reconnection rate at the magnetopause. The presence of high-density plasmaspheric plume material at the magnetopause causes transient reductions in the reconnection rate of up to ~40%.

Plain Language Summary As the solar wind propagates from the Sun to the Earth, it encounters two boundaries that limit its access to the near-Earth environment. The first is a bow shock that heats, slows, and deflects the solar wind. The second is the Earth's magnetopause, where the shocked solar wind is deflected around the Earth's magnetic field region called the magnetosphere. Magnetic reconnection at the magnetopause creates an interconnection between the magnetic field of the shocked solar wind and the Earth's magnetic field. The rate at which these magnetic fields interconnect, the reconnection rate, depends on the amount of plasma (ions and electrons) on either side of the magnetopause. This research uses observations from the Magnetospheric Multiscale mission to look at this rate for times when there is substantial plasma on the magnetospheric side of the magnetopause. These instances are rare; however, when they do occur, they reduce the reconnection rate by a substantial amount (up to 40%).

1. Introduction to Magnetospheric Plasma Populations at the Magnetopause

Since the discovery of an ionospheric source of plasma in the magnetosphere (Shelley et al., 1972), there has been extensive study of the implications for this plasma in the inner magnetosphere (e.g., Denton et al., 2019; Kronberg et al., 2014; and references therein). Studies of the importance of this plasma at the Earth's magnetopause using ion composition measurements are less numerous (e.g., Fuselier, Burch, et al., 2016; Fuselier et al., 2017, 2019; Wang et al., 2015).

At the dayside magnetopause, three primary ion populations are observed: the ring current, warm plasma cloak, and material from the plasmasphere and/or plasmaspheric drainage plume. The term plasmaspheric

drainage plume material is used here to identify plasma that is either directly associated with the plasmaspheric drainage plume, or has characteristics of drainage plume plasma without direct association with a plume. This material is observed across the dayside, with concentrations in the noon to dusk sector (Chappell, 1974; Fuselier et al., 2017; Lee et al., 2016).

These three ion populations in the dayside magnetosphere have different energies and composition. The ring current is a high-energy (tens of kiloelectron volt) population of both solar wind and ionospheric origin. It consists of H^+, He^{2+}, and high-charge-state Oxygen from the solar wind and H^+, O^+, and He^+ from the ionosphere (e.g., Kistler et al., 1989). The warm plasma cloak is a moderate-energy (tens of electron volt to several kiloelectron volt) population of ionospheric origin. It consists of H^+, O^+, and He^+, with O^+ as the dominant heavy ion (Chappell et al., 2008). Finally, the plasmaspheric drainage plume material is a low-energy (<1 eV to ~10s of eV) population also from the ionosphere. It consists of H^+, O^+, and He^+, with He^+ as the dominant heavy ion (e.g., Berube et al., 2005).

Surveys of these populations in the vicinity of the magnetopause revealed that they have a mass-loading effect at the boundary, which results in reduced reconnection efficiency (Borovsky & Denton, 2006, 2008; Fuselier et al., 2017, 2019; Su et al., 2000; Walsh et al., 2013; Walsh, Foster, et al., 2014; Walsh, Phan, et al., 2014; Wang et al., 2015). Alfvén speed changes induced by higher inflow mass densities into the reconnection region are expected to reduce the reconnection rate. Due to the square root dependence of the Alfvén speed on the mass density, a substantially large mass density is required for a dramatic decrease in the reconnection rate. Thus, the reduction of the reconnection rate is relatively modest most of the time. However, the magnitude of the reduction depends strongly on mass density, therefore it is strongly driven by the concentrations of heavy ionospheric ions. While the ring current has significant heavy ion concentrations, the total density of the ring current is typically <1 cm^{-3}, therefore its effect on reconnection is almost always very small.

Of the three ion populations, the warm plasma cloak often has the largest mass-loading effect on reconnection because of its high O^+ concentration and therefore its high mass density (Fuselier et al., 2019). However, in terms of number density, the plasmaspheric plume material has the highest density near the magnetopause, with densities in one instance approaching 100 cm^{-3} (Walsh, Foster, et al., 2014). To quantify the mass-loading effect of the plasmaspheric plume material on reconnection, it is necessary to include the He^+ concentration. This ion has concentrations from 1% to 10% of the dominant H^+ population (e.g., Berube et al., 2005; Reasoner et al., 1983). Therefore, He^+ contributes up to 40% of the mass density of the plume material at the magnetopause.

The purpose of this paper is to use observations from the MMS mission to quantify the maximum mass-loading effect of magnetospheric H^+ and He^+ on dayside magnetopause reconnection. Data from the Magnetospheric Multiscale (MMS) mission are used to identify magnetopause crossings with the highest He^+ concentrations. Section 2 describes the MMS mission and the magnetopause crossing selections. Section 3 discusses the results, including direct or indirect association of the observed He^+ with a model plasmaspheric plume. Section 4 quantifies the effect on reconnection, and Section 5 is a summary and discussion.

2. MMS Mission and Instrumentation

The four spacecraft in the MMS mission were launched in 2015 to use the near-Earth environment as a laboratory to study magnetic reconnection (Burch et al., 2016). The Earth's magnetopause and the magnetotail were the two regions of the magnetosphere that were targeted for these reconnection studies. In the first 2 years of science operations, from September 2015 to February 2017, the spacecraft apogees were 12 Earth Radii (R_E) and the spacecraft made two nearly complete sweeps of the dayside magnetopause from the dusk to dawn terminators. These two sweeps of the dayside magnetopause are called mission phases 1a and 1b (Fuselier, Lewis, et al., 2016). Half-way through phase 1a, there were 3,200 encounters with the magnetopause and ~1200 complete crossings reported (Petrinec et al., 2016). Through both phase 1a and 1b, there were more than 9,000 partial and complete magnetopause crossings, most with high data rate coverage. For nearly all of these crossings, the spacecraft were separated from each other by less than 60 km and, for the analysis here, data from a single spacecraft in the constellation is sufficient.

High data rate, that is, burst-mode, intervals from the two mission phases were used to create a data base of current-sheet crossings (Paschmann et al., 2018). This data base was later expanded to include some cur-

Table 1
High-Density He^+ Intervals at the Earth's Magnetopause[a]

Date	Magnetopause crossing time (hhmm:ss) UT; Local time of crossing (hh.h)	Average (mean) magneto-sheath mass density (cm^{-3}—amu)	Average, maximum He^+ density (cm^{-3})	Average, maximum magneto-spheric mass density (cm^{-3}—amu)	Direct association with plume? (Y or N)	Normalized reconnection rate Average He^+ density, maximum He^+ density
December 9, 2016	1756:32; 14.7	23.9	0.54, 1.2	41.1, 50.8	Y	0.68, 0.64
December 17, 2016	1633:12; 14.0	53.6	0.09, 0.72	12.8, 27.0	Y	0.92, 0.86
November 21, 2016	1914:54; 15.6	50.8	0.24, 0.36	20.4, 12.5	N	0.85, 0.90
October 2, 2015	0750:21; 14.3	19.8	0.27, 0.41	6.1, 9.1	Y	0.85, 0.77
December 26, 2016	1505:05; 13.4	18.1	0.05, 0.27	8.5, 17.6	N	0.90, 0.84
November 12, 2016	1837:11; 15.8	18.5	0.16, 0.23	7.6, 11.0	N	0.90, 0.86
November 22, 2016	1829:15; 15.4	28.5	0.27, 0.33	6.3, 8.0	Y	0.92, 0.89
November 22, 2016	1846:44; 15.4	22.2	0.06, 0.51	1.3, 12.9	Y	0.97, 0.80
September 18, 2015	0837:48; 14.9	42.2	0.37, 0.54	8.5, 12.7	Y	0.92, 0.89
November 9, 2016	2005:00; 16.2	82.9	0.18, 0.28	3.9, 6.2	N	0.99, 0.98
October 27, 2015	1243:42; 14.2	13.3	0.16, 0.27	3.5, 6.8	N	0.89, 0.82
January 26, 2017	1245:32; 11.7	80.0	0.17, 0.23	10.2, 16.7	N	0.96, 0.93
January 2, 2017	1444:17; 13.0	29.5	0.09, 0.11	17.5, 18.3	Y	0.85, 0.85
November 6, 2016	0915:08; 14.0	23.5	0.13, 0.19	2.6, 4.1	N	0.94, 0.90

[a]These are in order of the He^+ density, from highest to lowest as determined from the original current-sheet data base.

rent-sheet crossings from subsequent mission phases. However, the bulk of the data base consists of 8,670 burst-mode intervals from the first two mission phases. The data base contains observations from a single spacecraft (mostly MMS2) and from nearly all instruments on that spacecraft, including composition measurements from the Hot Plasma Composition Analyzer (HPCA) (Young et al., 2016). For each current-sheet crossing, the data base contains the type of current sheet and 80 scalar and vector parameters describing the current-sheet characteristics. Current-sheet types include the Earth's bow shock, partial and full magnetopause crossings, and current sheets in the solar wind and magnetosheath.

This data base was queried using Structured Query Language to select full magnetopause crossings and order these crossings by He^+ density on the magnetospheric side of the crossing. The ~25 crossings with He^+ densities >0.3 cm^{-3} were inspected by eye to eliminate crossings with significant contamination of the He^+ density from uncorrelated H^+ events in the HPCA time-of-flight (TOF) system. Although HPCA has a radio frequency (RF) system to reduce the H^+ flux (Young et al., 2016), there are still uncorrelated H^+ events that produce background across the entire HPCA TOF window, that is, across all masses. These uncorrelated H^+ events occur at energies where the H^+ flux is very high. High fluxes almost always occur in the magnetosheath, the magnetopause current layer (CL), and the boundary layers on either side of the magnetopause at energies between 0.1 and ~1 keV. The boundary layers are the magnetosheath boundary layer (MSBL) on the magnetosheath side of the magnetopause and the low latitude boundary layer (LLBL) on the magnetospheric side. Thus, He^+ densities in the data base are often contaminated to some degree by this background. After eliminating crossings with high background and combining crossings within 10 min of one another, 14 crossings remained. Observations within ~±10 min from the magnetopause crossings were used to determine magnetosheath and magnetospheric mass densities.

Parameters for these 14 crossings are shown in Table 1. The columns in Table 1 are the date, time, and local time of the magnetopause crossing, the average (mean) magnetosheath mass density, the average and maximum He^+ densities, the average (mean) and maximum magnetospheric mass densities, an indicator whether the crossing is directly associated with a plasmaspheric plume, cf. Section 3, and the normalized reconnection rate due to the presence of magnetospheric plasma, cf. Section 4. The crossings in Table 1

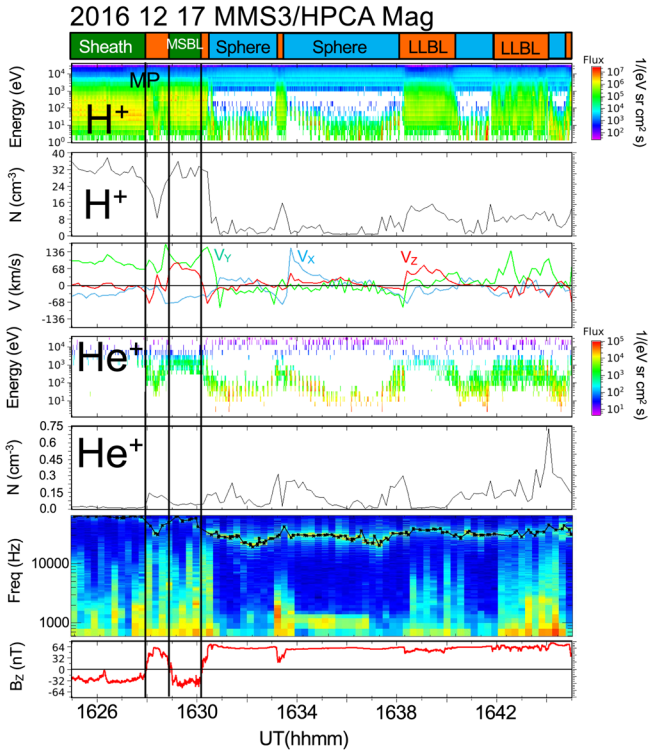

Figure 1. Magnetopause crossing on December 17, 2016 that had high He^+ density in the magnetosphere/LLBL. Top to bottom are a region identifier, the H^+ energy-time spectrogram, H^+ density, H^+ velocity components, He^+ spectrogram, He^+ density, plasma wave spectrogram, and B_Z component of the magnetic field. At the magnetopause crossings (vertical black lines), the field rotates from southward in the magnetosheath/MSBL to northward in the LLBL/magnetosphere. In the magnetosphere, there are two populations of H^+ and He^+, a high-energy ring current population and a lower-energy population of plasmaspheric plume material. The He^+ and H^+ densities in the magnetosphere vary dramatically as does the energy of the plasmaspheric plume material. The plasma frequency (black trace in the frequency-time spectrogram) remains high and has less variation in the magnetosphere, indicating that there is a significant population of cold ions that is not measured by the ion composition instrument. A 1.5-min interval from 1631 to 1632:30 and the peak He^+ density at 1644 UT were chosen to represent the average and maximum composition of the plasmaspheric plume material, respectively. LLBL, low latitude boundary layer; MSBL, magnetosheath boundary layer.

are listed in descending order of the He^+ density as reported in the current-sheet data base. The current-sheet data base uses measurements usually within 1 min of a magnetopause crossing, therefore Table 1 is approximately in descending order of the maximum He^+ density. However, because of background contamination discussed in the Section 3, some of the high He^+ densities for some crossings were reduced. Table 1 preserves the original ordering of the crossings in part to emphasize that care must be taken when using the HPCA data in general.

3. Survey Results and Association with Plasmaspheric Plume Material

There are some common characteristics of the 14 crossings in Table 1 that indicate that plasmaspheric plume material was present in the magnetosphere and boundary layers for all of the crossings. The magnetopause crossings in Table 1 almost all occurred on the duskside from ~12 to 16 h magnetic local time (LT). This duskside sector, from 12 to 18 LT, is also where the plasmaspheric drainage plume is observed (e.g., Chappell et al., 2008). Although the average O^+ densities are not shown in Table 1, they were all significantly lower than the average He^+ densities. In the plasmasphere and plume, the He^+ density is higher than the O^+ density (Berube et al., 2005; Fuselier et al., 2017; 2019). The average and maximum He^+ densities are considerably different, indicating that there is significant variability in the He^+ density near the magnetopause. Densities in the plasmaspheric plume are often highly variable (e.g., Spasojevic & Fuselier, 2009). Finally, only two of the 14 crossings, those on December 26, 2016 and October 27, 2015, were associated with geomagnetic storms, and these storms were relatively weak. The association with storms was determined using the list of geomagnetic storm days available at https://www.spaceweatherlive.com/en/auroral-activity/top-50-geomagnetic-storms. In contrast, the highest O^+ density, warm-plasma-cloak intervals in the magnetosphere were all associated with geomagnetic storms (using the same list of geomagnetic storms), and most of these storms were among the most intense for 2015–2017 (Fuselier et al., 2019). Plasmaspheric material is convected to the outer magnetosphere and magnetopause during times of enhanced magnetospheric convection. Enhanced convection may occur during geomagnetic storms; however, it does not require storm conditions (e.g., Nishida, 1975). Sustained intervals when the interplanetary magnetic field (IMF) is southward also produce enhanced convection.

Although these characteristics strongly suggest that plasmaspheric plume material was present at all magnetopause crossings, the last column in Table 1 indicates that only half of the crossings were directly associated with the plume. Two crossings are highlighted here to show how this association or lack of association with the plasmaspheric plume was determined and to also illustrate how densities and mass densities in the magnetosheath and in the magnetosphere were determined.

The first example magnetopause crossing occurred on December 17, 2016, and this crossing had the second-highest He^+ density of the data base. The IMF clock angle was 115°, indicating it was southward with a substantial Y component. Top to bottom panels in Figure 1 are a region identifier, H^+ energy-time flux spectrogram, H^+ density, three components of the H^+ velocity, He^+ flux spectrogram, He^+ density, plasma wave spectrogram, and B_{ZGSM} (Geocentric Solar Magnetospheric) component of the magnetic field. The spacecraft crossed the magnetopause three times, at 1628:00, 1629:00, and 1630:05 UT as shown by the black lines that are centered on the rotation of the magnetic field from south to north.

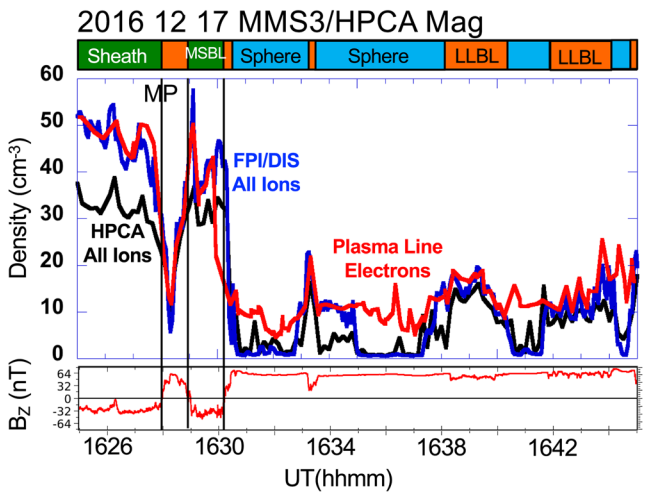

Figure 2. Plasma densities from HPCA, FPI/DIS, and derived from the plasma line for the 20-min interval in Figure 1. The top panel shows the region identifier and the bottom panel shows the B_Z component of the magnetic field from Figure 1 for context. In the magnetosheath/MSBL, the HPCA densities are lower than those from FPI/DIS and the plasma line because HPCA often saturates in the magnetosheath/MSBL. The three densities agree reasonably well in the LLBL; however, the HPCA and FPI/DIS densities are often much lower than those from the plasma line in the magnetosphere. The low-energy plasmaspheric ions are not adequately measured in the ion instruments. DIS, Dual Ion Spectrometer; FPI; Fast Plasma Investigation; HPCA, Hot Plasma Composition Analyzer; LLBL, low latitude boundary layer; MSBL, magnetosheath boundary layer.

In the magnetosheath at the beginning of the interval, the H^+ flux between 0.01 and ~1 keV is high. The spacecraft was at the duskside magnetopause near the ecliptic; therefore, the predominantly $+V_Y$ bulk flow of the magnetosheath plasma is consistent with the flow around the magnetospheric obstacle. In the MSBL there are relatively high-speed H^+ flows in the $+V_Z$ direction (antiparallel to the magnetic field), indicative of exhaust jets associated with magnetopause reconnection. In the LLBL, near the magnetopause crossing, the high-speed flows are in the $+V_Y$, $-V_Z$ direction (also antiparallel to the magnetic field). The flow direction in the boundary layer indicates the direction to the X-line (e.g., Fuselier et al., 2011). Antiparallel jetting in the MSBL indicates that the X-line was southward of the spacecraft while antiparallel jetting in the LLBL indicates that the X-line was northward of the spacecraft. Thus, during this set of crossings, a switch in the jet direction occurs, indicating proximity to the reconnection X-line (e.g., Trattner et al., 2018). Combined, these observations indicate that reconnection was occurring at the magnetopause during the interval and that the reconnection X-line passed near the spacecraft as it was crossing the magnetopause.

There are two plasma populations in the magnetosphere. The higher-energy (>1 keV) population is the ring current, and the lower-energy (<100 eV) population is the plasmaspheric plume material. The energy distinction between the two populations is evident for both H^+ and He^+. In the magnetosphere, the energy of the plasmaspheric material is variable, with the energy of the cold He^+ population higher than that of the cold H^+ population. The ordering of energy by mass indicates that these two cold populations are convecting with the same bulk velocity in the magnetosphere. This common convection velocity is confirmed from the velocity space distributions (not shown). The bulk velocity is variable and sometimes over 100 km/s.

For H^+, the highest densities are in the magnetosheath and MSBL; there are intermediate densities in the LLBL and lower densities in most of the magnetosphere intervals. For He^+, the densities are variable, and there is one high-density spike that occurs near the end of the interval in the magnetosphere near the earthward edge of the LLBL. This variable density in the magnetosphere is typical of plume material (Borovsky & Denton, 2008).

The plasma wave spectrogram shows a clear electron plasma oscillation (Langmuir wave) line throughout the interval (traced out with the black line in the panel). The waves could be at the upper hybrid frequency; however, the difference between the upper hybrid frequency and the plasma frequency is very small in the outer magnetosphere and magnetosheath. For electron plasma oscillations generated by electron beams with beam velocities much greater than plasma thermal velocities (e.g., Fuselier et al., 1985), the plasma frequency, f_p (in kHz), is related to the electron density, $n_e(cm^{-3})$ through the equation:

$$f_p \sim 9\sqrt{n_e} \quad (1)$$

The plasma line in Figure 1 traces out a different density profile from the H^+ and He^+ density profiles, and these differences underscore the cold nature of the plasmaspheric plume material and the complicated response of HPCA to cold and/or dense plasma.

Figure 2 shows the densities from HPCA, the Fast Plasma Investigation (FPI) Dual Ion Spectrometer (DIS), and from the plasma line for the 20-min interval in Figure 1. The HPCA "all ion" densities were obtained by summing the H^+, He^{2+}, He^+, and O^+ densities derived from the individual distributions. The FPI/DIS densities were direct from the instrument, assuming that all ions are protons. The wave densities were from the plasma line in Figure 1 and Equation 1. In the magnetosheath and the MSBL, FPI/DIS and wave densities agree reasonably well, while HPCA underestimates the density. In the LLBL, for example at 1638–1640 UT,

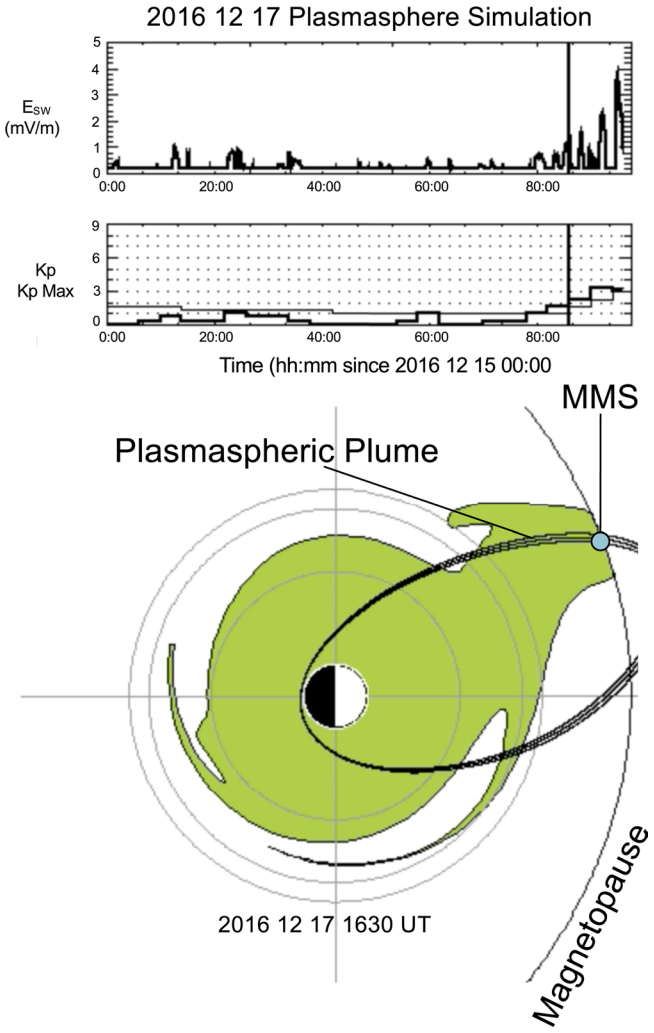

Figure 3. Plasmasphere and plasmaspheric plume simulation results for the magnetopause crossing in Figure 1. The simulation was started 3 days before the MMS magnetopause crossing and uses the electric field in the solar wind and the Kp index as input to drive a test-particle simulation. The green region is the plasmasphere and plume locations for the MMS magnetopause crossing. MMS crossed in the middle of the terminus of plasmaspheric plume at the magnetopause. MMS, Magnetospheric Multiscale.

the three densities agree reasonably well. In the magnetosphere, FPI/DIS and HPCA densities are most often much lower than the wave densities.

The H^+ density measured by HPCA in the magnetosheath and MSBL is lower than the electron density from the plasma line because the HPCA detector saturates in the high-density magnetosheath and MSBL. In the LLBL, the saturation is not as great, which is why the three densities agree. The H^+ densities from HPCA and FPI/DIS in the magnetosphere are often <1 cm^{-3}, for example from 1635 to 1636 UT, and the density is clearly correlated with the energy of the low-energy H^+ population.

HPCA often underestimates the cold plasma density in the magnetosphere by a factor of 10 or more because of two effects. First, the plasma population in the magnetosphere is so cold that it does not fill the field-of-view of an azimuthal angle-polar angle pixel in the HPCA instrument. As a result, H^+ and He^+ densities are underestimated by about a factor of 3 because the instrument geometric factor that is derived from laboratory calibration assumes that the flux fills the pixel uniformly (Toledo-Redondo et al., 2019; Young et al., 2016). Second, the energy of the cold population is often close to and below the ~1 eV minimum energy of HPCA, especially when the ~+4-V spacecraft potential is included. As a result, H^+ and He^+ densities in Figure 1 are underestimated by an additional factor of 3 or more, depending on how much of the cold, low-energy H^+ distribution does not make it through the positively charged sheath surrounding the spacecraft. There is an additional effect on cold beams due to the potential on electric field booms (Toledo-Redondo et al., 2019) that is not considered here because it is intermittent and mainly affects the FPI/DIS measurements. The determination of the mass densities in the magnetosheath and magnetosphere in Section 4 takes into account these instrument effects.

Figure 3 shows results from a simulation of the plasmaspheric plume for the magnetopause crossing in Figure 1. The plasmasphere and plasmaspheric plume boundaries were simulated in a plasmapause test-particle-tracing model (Goldstein et al., 2003; 2005). The dynamic locations of the boundaries were determined from a large number of cold test particles that are subject only to the **E x B** drift in a time-varying convection electric field. This simulation was initiated 3 days before the MMS magnetopause crossing in Figure 1 using 5-min averages of the observed solar wind from the OMNI data base to specify the electric field (see the top panel of Figure 3). Fine-scale features in the plume such as the long, thin region in the dawnside inner magnetosphere in Figure 3 are likely not real. However, despite its simplicity, the simulation has been shown to reproduce the large-scale structure and location of the plasmasphere and plasmaspheric drainage plume (Goldstein et al., 2003; 2005). In Figure 3, there is a fairly broad drainage plume on the duskside. MMS encountered the magnetopause in the middle of this plume, providing strong evidence that low-energy H^+ and He^+ plasma observed in the magnetosphere in Figure 1 are directly associated with the plume.

The second example magnetopause crossing occurred on November 21, 2016 and had the third-highest He^+ density of the data base. The IMF clock angle was 134°, indicating that the IMF was southward with a substantial positive Y component. Figure 4 shows HPCA and magnetic field observations from this crossing. The format and the panels are the same as those in Figure 1. The spacecraft made a single, relatively slow crossing of the magnetopause centered at about 1914 UT in Figure 4. In the LLBL, near the magnetopause crossing, the high-speed flows predominantly in the $-V_X$, $+V_Y$, direction are likely associated with large-scale convective flow. However, there is additional high-speed flow in the $-V_Z$ direction. This LLBL flow is consistent with a reconnection site northward and dawnward of the spacecraft.

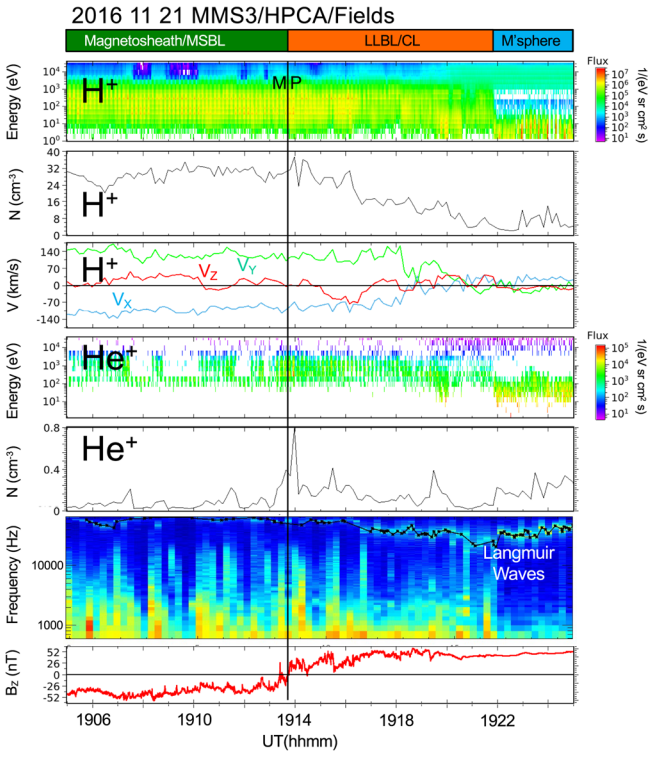

Figure 4. Magnetopause crossing on November 21, 2016. The format is the same as in Figure 1. There is significant He^+ in the magnetosheath/MSBL that is escaping the magnetosphere along reconnected field lines. The plasma frequency remains high, indicating that there is a significant population of cold ions in the magnetosphere that is not measured by the ion composition instrument. A 1-min interval from 1923:20 to 1924:20 UT and the peak He^+ density at 1914 UT, just after the magnetopause crossing, were chosen to represent the composition of the plasmaspheric plume material. MSBL, magnetosheath boundary layer.

There is a plasma line throughout the interval that provides an accurate measure of the electron density. Figure 5 shows the HPCA, FPI/DIS, and plasma line derived densities for the 20-min interval in Figure 4. The format for Figure 5 is the same as that for Figure 2. Once again, in the magnetosheath, HPCA underestimates the density because of saturation effects. FPI/DIS densities are sometimes higher than those determined from the plasma line because the plasma line is near the maximum frequency of the wave measurement. In the LLBL/CL, the densities agree well when the total density is less than about 20 cm^{-3}. In the magnetosphere, the plasma line derived densities are always higher than the HPCA and FPI/DIS densities because of the presence of a large number of low-energy ions.

In Figure 4, there is a nearly continuous line of He^+ flux in the magnetosheath and MSBL at about 100 eV. This is not He^+ flux, rather it is the background H^+ bleed-over into the He^+ (and other ion) time-of-flight channels. The sharp cutoff in this background >100 eV is due to the HPCA RF system's reduction of the proton flux and therefore reduction in the bleed-over background in other time-of-flight channels. Thus, He^+ fluxes above this sharp cutoff are not background. Instead, they are a He^+ population escaping from the magnetosphere along reconnected field lines that thread the open magnetopause. In the LLBL and magnetosphere, the H^+ fluxes are lower, and there is no bleed-over background in the He^+ spectrogram. Immediately after crossing the magnetopause, there is a spike in the He^+ density for a single, 10-s measurement. Inside the LLBL and in the magnetosphere, the He^+ flux and density are variable, due to variations in the cold plasmaspheric material in these regions.

Figure 6 shows results from the simulation of the plasmaspheric plume for the magnetopause crossing in Figure 4. The simulation setup was the same as the one for the magnetopause crossing in Figure 1 and the format of Figure 6 is the same as that in Figure 3. Unlike the crossings in Figure 3, the magnetopause crossing in Figure 6 occurred several Earth Radii from the predicted location of the plasmaspheric plume at the magnetopause. Despite this, Figure 4 shows there is clearly high-density plasmaspheric material in the LLBL from 1914 to 1922 UT and in the adjacent magnetosphere from 1922 to 1925 UT.

The contrast between the plasmasphere simulation in Figures 3 and 6 emphasizes the difference between a crossing that is directly associated with a plume (Figure 3) and a crossing that is not directly associated with a plume (Figure 6). Simulations like the ones shown in Figures 3 and 6 were run for all of the 14 crossings in Table 1. The seven crossings that occur within a plume (see Figure 3) or within ~1 R_E of a plume are identified as "directly associated with a plume." The other seven crossings in Table 1 occurred several R_E from the predicted plume (see Figure 6).

4. Effect on Reconnection

Cassak and Shay (2007) and Birn et al. (2008) proposed corrections to the reconnection rate due to the presence of magnetospheric plasma. Defining a reconnection rate = 1.0 when no magnetospheric plasma is present, Equation 2 (Borovsky et al., 2013; Fuselier, Burch, et al., 2016) is the reduced rate due to the presence of magnetospheric plasma.

$$R = \left(1 + \mathrm{MC}\right)^{-\frac{1}{2}} \tag{2}$$

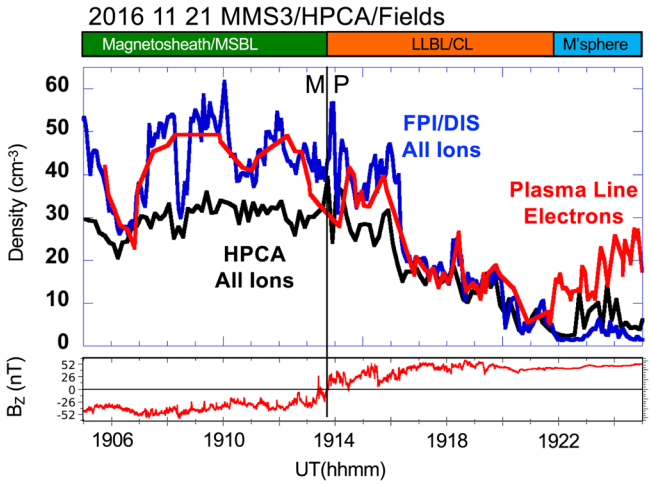

Figure 5. Plasma densities from HPCA, FPI/DIS, and derived from the plasma line for the 20-min interval in Figure 4. The format is the same as in Figure 2. As in Figure 2, the HPCA densities are lower than those from FPI/DIS and the plasma line in the magnetosheath/MSBL because HPCA often saturates in the magnetosheath/MSBL. The three densities agree reasonably well in the LLBL; however, the HPCA and FPI/DIS densities are often much lower than those from the plasma line in the magnetosphere. The low-energy plasmaspheric ions are not adequately measured in the ion instruments. DIS, Dual Ion Spectrometer; FPI; Fast Plasma Investigation; HPCA, Hot Plasma Composition Analyzer; LLBL, low latitude boundary layer; MSBL, magnetosheath boundary layer.

here, MC is the mass correction factor defined as:

$$\mathrm{MC} = \frac{\rho_M\, B_S}{\rho_S\, B_M} \tag{3}$$

where ρ_M and ρ_S are the mass densities in the magnetosphere and magnetosheath, respectively, and B_M and B_S are the magnetic field magnitudes in the magnetosphere and magnetosheath, respectively. The total field magnitude is used instead of the reconnecting component because Equations 2 and 3 represent a general, theoretical calculation of the normalized reconnection rate and the presence or absence of a guide field is not necessarily known.

While the mass density in the magnetosheath is reasonably well defined and relatively stable, no single value represents the highly variable densities and mass densities in the magnetosphere. Furthermore, there are instrument effects that produce apparent density variations that depend on the temperature and energy of the cold, magnetospheric population. Therefore, consistent with previous analyses of the effects of magnetospheric plasma on magnetic reconnection (Fuselier, Burch, et al., 2016; Fuselier et al., 2017, 2019), the magnetospheric mass density is represented by two values, an average mass density over an appropriate time interval in the magnetosphere and a peak mass density.

Because HPCA underestimates the H^+ density in the magnetosphere due to the low temperature and low energy of the plasmaspheric material, the mass density cannot be computed using HPCA measurements alone. Instead, HPCA composition measurements are used to determine the heavy ion concentrations, while the FPI and the plasma wave measurements are used to determine total ion and electron densities in the various plasma regions. The mass densities in the magnetosheath and magnetosphere are computed using a three-step process.

Some 20-min time periods surrounding a magnetopause crossing did not contain a magnetospheric interval with sufficiently high He^+ energy. For these periods, an interval in the LLBL was chosen. The LLBL intervals require an additional assumption in Step 2 to determine the magnetospheric H^+ density because H^+ in these intervals is from both solar wind and magnetospheric sources.

For the peak mass density, the highest He^+ density measured in the 20-min interval was selected. For example, Figure 1 uses the peak at 1644 UT, and Figure 4 uses the peak at 1914 UT. This peak density often occurred in the LLBL.

$$\rho_M = \frac{n_{e\text{-}}\, m_{H+}}{\left(1 + C_{He+} + C_{O+}\right)}\left(1 + 4C_{He+} + 16C_{O+}\right) \tag{4}$$

Because HPCA also underestimates the H^+ density in the magnetosheath due to saturation effects, a similar equation was used to determine the magnetosheath mass density:

$$\rho_S = \frac{n_{FPI}\, m_{H+}}{\left(1 + C_{He2+}\right)}\left(1 + 4C_{He2+}\right) \tag{5}$$

here, n_{FPI} is the ion density measured by the Fast Plasma Instrument, which does not saturate in the magnetosheath. C_{He2+} is the average He^{2+} concentration in the magnetosheath computed from the He^{2+} and H^+ densities from HPCA. The ion density is used instead of the electron density derived from the wave measurements because the highest wave frequency of 60 kHz corresponds to a density of 44 cm^{-3}, and the magnetosheath density was sometimes greater than this upper limit. Equation 5 assumes that the saturation in the HPCA instrument in the magnetosheath affects H^+ and He^{2+} equally and, in Equations 4 and 5, m_{H+}, is the proton mass.

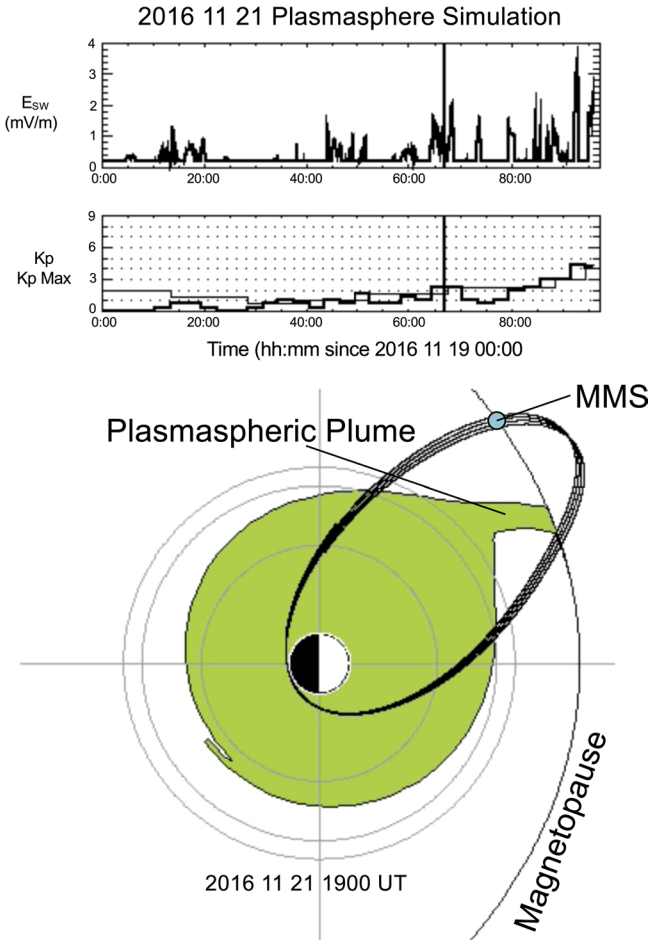

Figure 6. Plasmasphere and plasmaspheric plume simulation results for the magnetopause crossing in Figure 3. MMS crossed the magnetopause far away from the plasmaspheric plume at the magnetopause. MMS, Magnetospheric Multiscale.

Table 1 shows the average and peak mass densities in the magnetosphere and the average mass density in the magnetosheath determined from Equations 4 and 5, respectively. For the first crossing listed in Table 1, the average mass density in the magnetosheath is less than the average and peak mass densities in the magnetosphere. For all other crossings, the opposite is true. Although not shown, the magnetic field magnitude in the magnetosheath is usually less than that in the magnetosphere, although the difference is usually relatively small. However, this lower magnetic field magnitude in the magnetosheath further reduces the mass correction factor in Equation 2. Thus, excluding the crossing with the highest He^+ density, the mass correction factor in Equation 2 is relatively small, and the reduction in the reconnection rate in Equation 2 is relatively modest.

Figure 7 shows the theoretical reductions in the average (left panel) and peak (right panel) reconnection rate due to the presence of high-density plasmaspheric material at the magnetopause. The left panel shows that there is only modest reduction in the reconnection rate when the average mass density of the plasmaspheric plume material is used in Equation 4. The right panel shows that the reduction in the rate is typically larger when the peak mass density is used, indicating that transient changes in the reconnection rate are often larger. However, even these transient changes amount to a reduction of ~40% in one crossing only. The average reduction for this event was ~35% and these reductions are much larger than the typical reduction of ~10–15%.

5. Summary and Conclusions

A data base of current-sheet crossings from the first two years of the MMS mission was used to select full magnetopause crossings with the highest He^+ densities in the magnetosphere/LLBL. Ultimately, 14 crossings, profiled in Table 1, were selected from the ~25 crossings with the highest He^+ density. These crossings all had several features in common, and these features indicate that plasmaspheric plume material was observed in the magnetosphere/LLBL for these crossings.

All crossings occurred between about 12 and 16 Local Time, or at the dusk magnetopause where the plasmaspheric plume and plume material are commonly observed (e.g., Chappell et al., 2008; Fuselier et al., 2017). The He^+ density in the magnetosphere was higher than the O^+ density, consistent with plasmaspheric material and inconsistent with the warm plasma cloak (Fuselier et al., 2017). Finally, only two of the 14 crossings were associated with geomagnetic storms, and the storms were relatively weak. Convecting plasmaspheric plume material to the magnetopause requires enhanced magnetospheric convection. This enhanced convection occurs when the IMF is southward for a sustained time interval, and these southward IMF intervals do not need to be associated with geomagnetic storms. In contrast, the highest O^+ densities at the dayside magnetopause all occurred when the warm plasma cloak was in the vicinity of the magnetopause during fairly strong geomagnetic storms (Fuselier et al., 2019).

Although plasmaspheric material was present at all crossings, Table 1 shows that only seven of 14 crossings were directly associated with a model plasmaspheric plume. Two of the 14 events were showcased in Figures 1–6. The first event, in Figures 1–3, was associated with a plasmaspheric plume. The second event, in Figures 4–6, was not associated with a plume. In the second event, Figure 6 shows that MMS was several R_E duskward of the predicted plume location. Magnetic reconnection at the magnetopause and subsequent convection of reconnected plasma in the LLBL may result in transport of plasmaspheric plume material from the plume location to the MMS spacecraft. Figure 8 shows a schematic of this process. In Figure 8, the location of the MMS spacecraft relative to the plume is shown as in Figure 6. Added to this geometry

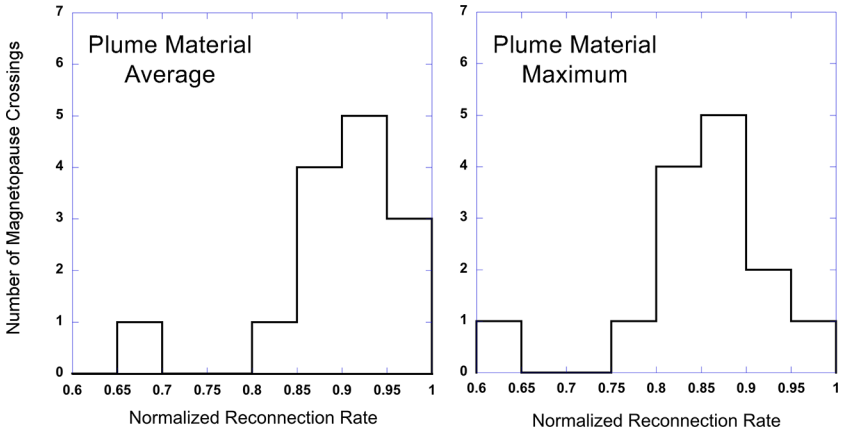

Figure 7. Normalized reconnection rates for the 14 magnetopause crossings in Table 1 using the average mass densities of the plume material (left panel) and the maximum mass densities of the plume material (right panel). Plasmaspheric plume material has a modest effect on the reconnection rate at the magnetopause, reducing the rate by ~10% when the average mass densities are used and about 13% when the maximum mass densities are used. The one crossing with the highest reduction in the reconnection rate had the highest He^+ densities and is the first crossing listed in Table 1.

in Figure 8 is the location of a reconnection site that is closer to 12 Local Time. In three dimensions, the reconnection site is located northward and dawnward of the spacecraft location. If the plume is between the reconnection site and the MMS spacecraft, then convection of reconnected field lines in the LLBL will result in duskward convection of plasmaspheric plume material. In Figure 4 at 1914 UT, the >100 km/s $-V_X$, $+V_Y$ convection velocity in the LLBL is consistent with fast, tailward/duskward convection of reconnected field lines. Thus, the spike in the He^+ density at 1914 UT in Figure 4 could be the result of transport of plasmaspheric plume material from the plume to the MMS spacecraft. However, this same process does not explain the high He^+ densities in the magnetosphere, for example in Figure 4 from 1922 to 1924 UT. The convection velocity in the magnetosphere is <20 km/s and has a slight dawnward direction. Therefore, it is clear that there is significant plasmaspheric material near or at the dayside magnetopause that is not associated with a plume. The composition measurements confirm that material is clearly from the plasmasphere, but how it arrived at the MMS location is not known.

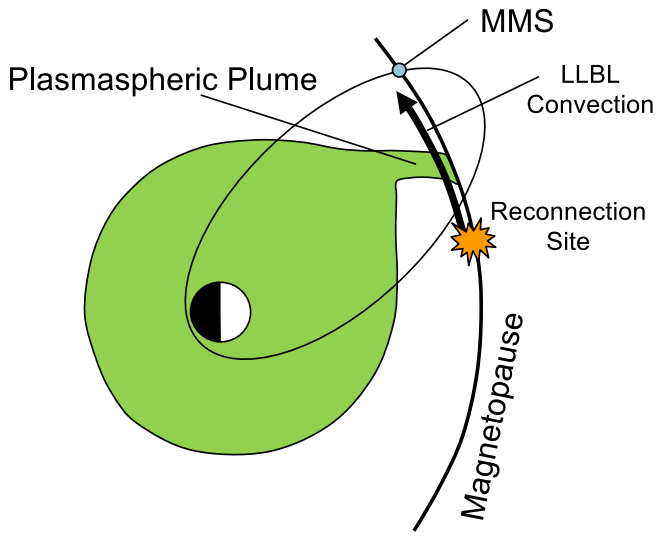

Figure 8. Scenario for convecting plasmaspheric plume material to the MMS spacecraft in the LLBL. A reconnection site that is closer to 12 Local Time creates high-speed bulk flow in the LLBL. The plume, between this reconnection site and the spacecraft, is swept up in this bulk flow and convected to the MMS spacecraft in the LLBL. LLBL, low latitude boundary layer; MMS, Magnetospheric Multiscale.

Figure 7 shows that the reconnection rate for these 14 magnetopause crossings is reduced only modestly due to the presence of the plasmaspheric material. For 13 of the crossings, there is about a 10% reduction in the normalized reconnection rate for the average mass density of the plume material and a 13%–15% transient reduction for the maximum mass density. One crossing, the first one in Table 1, had magnetospheric mass densities that were greater than the mass density in the magnetosheath for both the average and maximum magnetospheric mass densities. For this crossing, the reconnection rate was reduced by 33% for the average mass density and 37% for the maximum reconnection rate.

One mitigating factor in this overall result is that these observations were made during the declining phase of a fairly weak solar cycle. Thus, the importance of ionospheric material in magnetospheric dynamics is reduced because ionospheric outflow is proportional to solar activity. Furthermore, relatively weak solar activity translates into weak convection in the magnetosphere and therefore weak transport of plasmaspheric material to the dayside magnetopause. The expectation for the future is that the MMS mission will continue to observe modest, transient effects on the reconnection rate as the solar cycle declines and begins to increase. That said, there are two aspects of this study that point to an increased

importance of magnetospheric plasma in reconnection at the dayside magnetopause. The first is that the crossing with the highest He^+ density and the highest reduction in the reconnection rate demonstrates the potential for plasmaspheric material to influence reconnection. This is the only magnetopause crossing in the studies of the MMS composition data to date (Fuselier, Burch, et al., 2016; Fuselier et al., 2017, 2019) where the mass density in the magnetosphere was much higher than that in the magnetosheath. The second aspect of this study is that significant concentrations of plasmaspheric material do not appear to be confined to a narrow range of local times associated with the plasmaspheric plume at the magnetopause. Therefore, magnetospheric plasma, and, in particular, plume material may influence dayside reconnection over a much broader range of local times.

Data Availability Statement

The entire MMS data base is available online at https://lasp.colorado.edu/mms/sdc/public/Solar wind data from the OMNI data set at the CDAWeb (https://cdaweb.sci.gsfc.nasa.gov). Research at SwRI was supported by NASA contract NNG04E99C and NASA grant 80NSSC19K1107. P. Tenfjord received support from the Research Council of Norway under contract 300865.

Acknowledgments
The authors acknowledge support from two teams from the International Space Science Institute (ISSI): the "Study of the physical processes in magnetopause and magnetosheath current sheets using a large MMS data base" team (team 442) lead by Goetz Paschmann and Tai Phan, and the "cold ions" team (team 447) lead by Sergio Toledo-Redondo. ISSI, the entire MMS science team, and in particular the HPCA team provided a forum for presenting and discussing results from the mission. The MMS mission has been a tremendous success, and the many women and men that helped create this mission share in this success.

References

Berube, D., Moldwin, M. B., Fung, S. F., & Green, J. L. (2005). A plasmaspheric mass density modal and constraints on its heavy ion composition. *Journal of Geophysical Research*, *110*, A04212. https://doi.org/10.1029/2004JA010684

Birn, J., Borovsky, J. E., & Hesse, M. (2008). Properties of asymmetric magnetic reconnection. *Physics of Plasmas*, *15*(3), 032101. https://doi.org/10.1063/1.2888491

Borovsky, J. E., & Denton, M. H. (2006). The effect of plasmaspheric drainage plumes on solar-wind/magnetosphere coupling. *Geophysical Research Letters*, *33*, L20101. https://doi.org/10.1029/2006GL026519

Borovsky, J. E., & Denton, M. H. (2008). A statistical look at plasmaspheric drainage plumes. *Journal of Geophysical Research*, *113*, A09221. https://doi.org/10.1029/2007JA012994

Borovsky, J. E., Denton, M. H., Denton, R. E., Jordanova, V. K., & Krall, J. (2013). Estimating the effects of ionospheric plasma on solar wind/magnetosphere coupling via mass loading of dayside reconnection: Ion-plasma-sheet oxygen, plasmaspheric drainage plumes, and the plasma cloak. *Journal of Geophysical Research: Space Physics*, *118*, 5695–5719. https://doi.org/10.1002/jgra.50527

Burch, J. L., Moore, T. E., Torbert, R. B., & Giles, B. L. (2016). Magnetospheric multiscale overview and science objectives. *Space Science Reviews*, *199*(1-4), 5–21. https://doi.org/10.1007/s11214-015-0164-9

Cassak, P. A., & Shay, M. A. (2007). Scaling of asymmetric magnetic reconnection: General theory and collisional simulations. *Physics of Plasmas*, *14*, 102114. https://doi.org/10.1063/1.2795630

Chappell, C. R. (1974). Plasma regions in the magnetosphere. *Journal of Geophysical Research*, *79*, 1861.

Chappell, C. R., Huddleston, M. M., Moore, T. E., Giles, B. L., & Delcourt, D. C. (2008). Observations of the warm plasma cloak and an explanation of its formation in the magnetosphere. *Journal of Geophysical Research: Space Physics*, *113*, A09206. https://doi.org/10.1029/2007ja012945

Denton, M. H., Henderson, M. G., Maruyama, N., & Fuselier, S. A. (2019). The cold ion population at geosynchronous orbit and transport to the dayside magnetopause: September 2015 to February 2016. *Journal of Geophysical Research: Space Physics*, *124*, 8685–8694. https://doi.org/10.1029/2019JA026973

Fuselier, S. A., Burch, J. L., Cassak, P. A., Goldstein, J., Gomez, R. G., Goodrich, K. et al. (2016). Magnetospheric ion influence on magnetic reconnection at the duskside magnetopause. *Geophysical Research Letters*, *43*(4), 1435–1442. https://doi.org/10.1002/2015gl067358

Fuselier, S. A., Burch, J. L., Mukherjee, J., Genestreti, K. J., Vines, S. K., Gomez, R., et al. (2017). Magnetospheric ion influence at the dayside magnetopause. *Journal of Geophysical Research: Space Physics*, *122*(8), 8617–8631. https://doi.org/10.1002/2017ja024515

Fuselier, S. A., Mukherjee, J., Denton, M. H., Petrinec, S. M., Trattner, K. J., Toledo-Redondo, S. et al. (2019). High-density O+ in Earth's outer magnetosphere and its effect on dayside magnetopause magnetic reconnection. *Journal of Geophysical Research: Space Physics*, *124*(12), 10257–10269. https://doi.org/10.1029/2019ja027396

Fuselier, S. A., Gurnett, D. A., & Fitzenreiter, R. J. (1985). The downshift of electron plasma oscillations in the electron foreshock region. *Journal of Geophysical Research*, *90*, 3935–3946.

Fuselier, S. A., Lewis, W. S., Schiff, C., Ergun, R., Burch, J. L., Petrinec, S. M., & Trattner, K. J. (2016). Magnetospheric Multiscale science emission profile and operations. *Space Science Reviews*, *199*, 77–103. https://doi.org/10.1007/s11214-014-0087-x

Fuselier, S. A., Trattner, K. J., & Petrinec, S. M. (2011). Antiparallel and component reconnection at the dayside magnetopause. *Journal of Geophysical Research*, *116*, A10227. https://doi.org/10.1029/20011JA016888

Goldstein, J., Sandel, B. R., Forrester, W. T., Thomsen, M. F., & Hairston, M. R. (2005). Global plasmasphere evolution 22-23 April 2001. *Journal of Geophysical Research*, *110*, A12218. https://doi.org/10.1029/2005JA011282

Goldstein, J., Sandel, B. R., Reiff, P. H., & Hairston, M. R. (2003). Control of plasmaspheric dynamics by both convection and sub-auroral polarization stream. *Geophysical Research Letters*, *30*(24), 2243. https://doi.org/10.1029/2003GL018390

Kistler, L. M., Ipavich, F. M., Hamilton, D. C., Gloeckler, G., Wilken, B., Kremser, G., & Stüdemann, W. (1989). Energy spectra of major ion species in the ring current during geomagnetic storms. *Journal of Geophysical Research*, *94*(A4), 3579–3599. https://doi.org/10.1029/JA094iA04p03579

Kronberg, E. A., Ashour-Abdalla, M., Dandouras, I., Delcourt, D. C., Grigorenko, E. E., Kistler, L. M., et al. (2014). Circulation of heavy ions and their dynamical effects in the magnetosphere: recent observations and models. *Space Science Reviews*, *184*(1-4), 173–235. https://doi.org/10.1007/s11214-014-0104-0

Lee, S. H., Zhang, H., Zong, Q.-G., Otto, A., Rème, H., & Liebert, E. (2016). A statistical study of plasmaspheric plumes and ionospheric outflows observed at the dayside magnetopause. *Journal of Geophysical Research: Space Physics*, *121*, 492–506. https://doi.org/10.1002/2015JA021540

Nishida, A. (1975). Interplanetary field effect on the magnetosphere. *Space Science Reviews*, *17*, 353–359.

Paschmann, G., Haaland, S. E., Phan, T. D., Sonnerup, Burch, J. L., Torbert, R. B., et al. (2018). Large-scale survey of the structure of the dayside magnetopause by MMS. *Journal of Geophysical Research: Space Physics*, *123*, 2018–2033. https://doi.org/10.1002/2017JA025121

Petrinec, S. M., Burch, J. L., Fuselier, S. A., Gomez, R. G., Lewis, W., Trattner, K. J., et al. (2016). Comparison of Magnetospheric Multiscale ion jet signatures with predicted reconnection site locations at the magnetopause. *Geophysical Research Letters*, *43*(12), 5997–6004. https://doi.org/10.1002/2016gl069626

Reasoner, D. L., Craven, P. D., & Chapell, C. R. (1983). Characteristics of low-energy plasma in the plasmasphere and plasma trough. *Journal of Geophysical Research*, *88*, 7913–7925.

Shelley, E. G., Johnson, R. G., & Sharp, R. D. (1972). Satellite observations of energetic heavy ions during a geomagnetic storm. *Journal of Geophysical Research*, *77*, 6104–6110. https://doi.org/10.1029/JA077i031p06104

Spasojevic, M., & Fuselier, S. A. (2009). Temporal evolution of proton precipitation associated with the plasmaspheric plume. *Journal of Geophysical Research*, *114*, A12201. https://doi.org/10.1029/2009JA014530

Su, Y.-J., Borovsky, J. E., Thomsen, M. F., Elphic, R. C., & McComas, D. J. (2000). Plasmaspheric material at the reconnecting magnetopause. *Journal of Geophysical Research*, *105*, 7591–7600. https://doi.org/10.1029/1999JA000266

Toledo-Redondo, S., Lavraud, B., Fuselier, S. A., André, M., Khotyaintsev, Yu. V., Nakamura, R., et al. (2019). Electrostatic spacecraft potential structure and wake formation effects for characterization of cold ion beams in the Earth's magnetosphere. *Journal of Geophysical Research: Space Physics*, *124*(12), 10048–10062. https://doi.org/10.1029/2019ja027145

Trattner, K. J., Burch, J. L., Cassak, P. A., Ergun, R., Eriksson, S., Fuselier, S. A., et al. (2018). The transition between antiparallel and component magnetic reconnection at Earth's dayside magnetopause. *Journal of Geophysical Research: Space Physics*, *123*(12), 10177–10188. https://doi.org/10.1029/2018ja026081

Walsh, B. M., Foster, J. C., Erickson, P. J., & Sibeck, D. G. (2014). Simultaneous ground- and space-based observations of the plasmaspheric plume and reconnection. *Science*, *343*, 1122–1125.

Walsh, B. M., Phan, T. D., Sibeck, D. G., & Souza, V. M. (2014). The plasmaspheric plume and magnetopause reconnection. *Geophysical Research Letters*, *41*, 223–228. https://doi.org/10.1002/2013GL058802

Walsh, B. M., Sibeck, D. G., Nishimura, Y., & Angelopoulos, V. (2013). Statistical analysis of the plasmaspheric plume at the magnetopause. *Journal of Geophysical Research: Space Physics*, *118*, 4844–4851. https://doi.org/10.1002/jgra.50458

Wang, S., Kistler, L. M., Mouikis, C. G., & Petrinec, S. M. (2015). Dependence of the dayside magnetopause reconnection rate on local conditions. *Journal of Geophysical Research: Space Physics*, *120*(8), 6386–6408. https://doi.org/10.1002/2015ja021524

Young, D. T., Burch, J. L., Gomez, R. G., De Los Santos, A., Miller, G. P., Wilson, P., et al. (2016). Hot plasma composition analyzer for the magnetospheric multiscale mission. *Space Science Reviews*, *199*(1-4), 407–470. https://doi.org/10.1007/s11214-014-0119-6